# Scale-up for

***Manipulators with guidance constructions based on elastic mechanisms are of interest for the increasing number of precision vacuum applications. Previously, the design of an elastic MEMS-based 6-DOFs manipulator was presented. Characterization in six degrees of freedom (DOFs) of a manipulator the size of several square millimeters, however, is difficult. Therefore, a scaled-up version of the manipulator was built. This 'macro' version serves as a research platform for the verification of the flexible multi-body model including control that was set up using the SPACAR toolbox for Matlab.***

• *Martijn Huijts, Dannis Brouwer and Johannes van Dijk* •

For sample manipulation inside a confined space a Micro Electro-Mechanical Systems (MEMS)-based multi-DOFs manipulation stage is being researched [1]. The purpose of the manipulator is to position small samples (10 x 20 x 0.2 $\mu m^3$) in, for example, a Transmission Electron Microscope (TEM). MEMS offers the opportunity for downscaling, because of the confined space inside a TEM. Such a small in-situ manipulator would be of great advantage, because of the absence of having a distance (TEM typically 100 mm) between the sample and the manipulator, with all the jeopardized positional stability due to vibrations and heat influences involved. The time needed to create stable images would therefore be reduced seriously, which implies an improved operational time of the TEM.

Amongst others, the main criteria given for this manipulator are manipulation with a range of motion in three DOFs translations of tens of microns and three DOFs rotations of up to five degrees. The lowest vibration mode frequency should be higher than 1 kHz, taking into account the (very small) sample load. To obtain a good positioning repeatability, the mechanism design is based on exact constraint design [2] and the motion is realised by deformation of elastic parts, such as leaf-springs [3]. Real hinges would introduce backlash and friction, which would negatively influence accurate positioning and obstruct the repeatability of manipulator positioning.

Due to the small size and the 6-DOFs motion of this system a model is difficult to validate with experiments. Therefore, a scaled-up version, which was magnified roughly 100 times, was fabricated. The purpose of this set-up is the validation of a model-based control system design which will later also be applied for the MEMS manipulator. This set-up should resemble the behaviour of the MEMS-based manipulator. To this end, the characteristics of this manipulator, with the restrictions resulting from MEMS fabrication methods, were preserved, such as the parallel kinematic elastic mechanism with all the actuators in one (horizontal) plane and the asymmetric layout of the leaf-springs at the end-effector, which originates from the crystallographic orientation of single crystal silicon. Furthermore, a typical MEMS-based aspect ratio was used for the leaf-springs. The width/length ratio of the in-plane leaf-springs for example is approximately 1/10. More details about these ratios can be found in [1].

# model verification

## Design

The scaled-up configuration consists of only five elastic parts, which are clamped together at points indicated by dashed circles in the centre of Figure 1. All five parts were wire spark eroded out of one piece, to reduce the effects of internal stress [4] and to minimize hysteresis.

This manipulator mechanism was based on a proper choice of actuated and released DOFs as is pointed out in Figure 2. This was done by a combination of stiffnesses and masses such that there is a discrepancy between the low-frequency first six actuation-related modes and the seventh and higher high-frequency deformation modes.

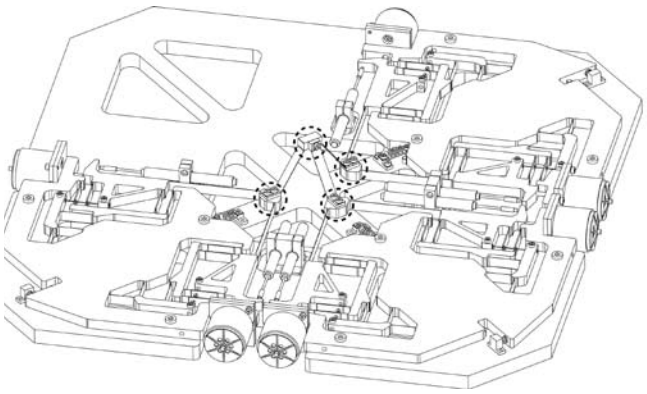

Figure 1. Scaled-up configuration with clamped points indicated by dashed circles.

As can be seen in Figure 2a, each intermediate body is connected by two perpendicularly placed in-plane leaf-springs. They ensure one compliant degree of freedom of the intermediate body, namely the rotation around the global z-axis (out-of-plane direction). The in-plane leaf-springs are actuated in the longitudinal direction resulting in two DOFs at the intermediate body. The remaining three DOFs are constrained by the high stiffness of the leaf-springs. Each slanted leaf-spring releases another three DOFs at the end-effector. One intermediate body together with a slanted leaf-spring will now ensure an actuation of the end-effector in two DOFs, while the other four DOFs are compliant. In total three of these intermediate bodies are connected to the end-effector by slanted leaf-springs, as shown in Figure 2b. In total this allows actuation in all six DOFs of the end-effector.

At the actuator part, shown in Figure 2c, the in-plane leaf-springs are connected to a straight guidance, which is actuated by a voice-coil actuator. This straight guidance leaves only the actuated direction free, while the other five DOFs are suppressed. Besides the thickened and therefore reinforced leaf-springs, the cantilever is added to improve the stiffness in the x-direction [1]. This cantilever pivots around an elastic hinge created by two leaf-springs. A wire flexure through the thickened part of one of the inner and one of the outer leaf-springs makes this lever mechanism complete.

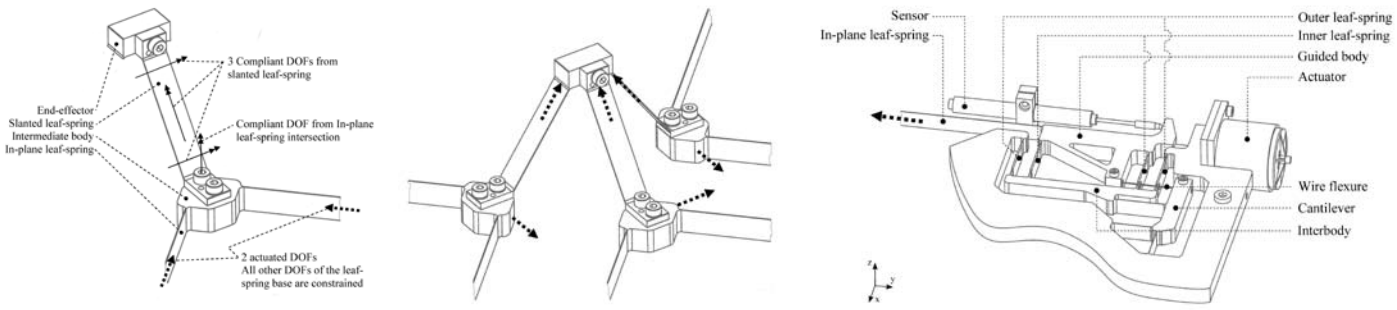


a b c

Figure 2. DOF selection for the manipulator mechanism.
(a) The four compliant DOFs and two actuated DOFs of the end-effector realized by one slanted leaf-spring connection.
(b) Two actuated DOFs per slanted leaf-spring resulting in six actuated DOFs of the end-effector.
(c) The actuator with guidance.

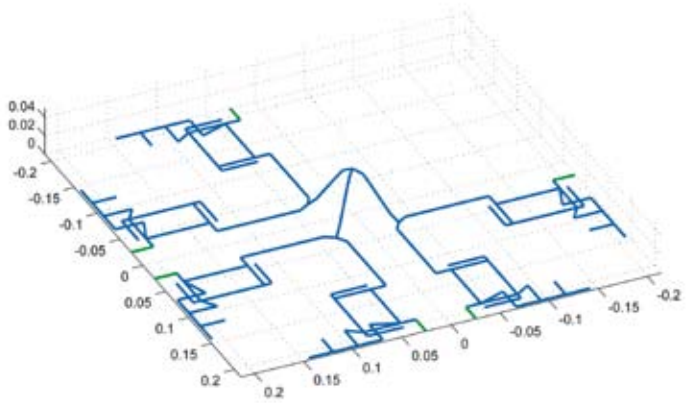

Figure 3. SPACAR model.

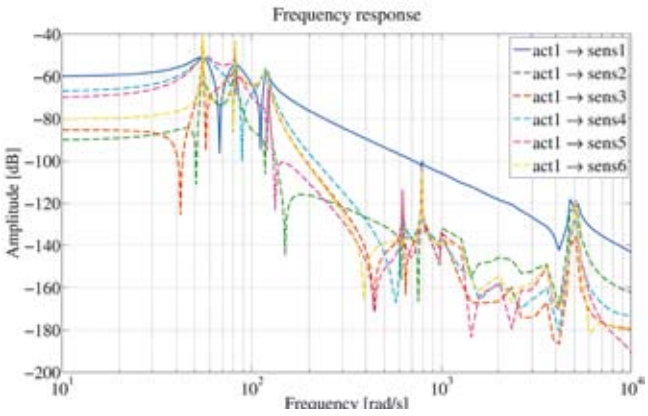


Figure 4. Transfers between actuator force and displacement as obtained by SPACAR.

## Modeling in SPACAR

The displacements of the elastic elements are relatively large, and because there is no sensor that measures the movements of the end-effector itself in six DOFs, an accurate modeling method is required, that describes the non-linear kinematic relations between the actuator and end-effector movements. This model, shown in Figure 3, was built using a multibody systems approach that is implemented in the SPACAR toolbox for Matlab [5]. This toolbox is based on a non-linear finite element description of flexible multibody systems [6].

With this model, the dynamics were analyzed. As can be seen in Table 1, the first six eigenfrequencies, hereafter called actuation-related modes, can be found in the region 50-125 rad/s. The next three eigenfrequencies are located in the region of 650-1,000 rad/s and the higher frequencies are just above 1,000 rad/s. Ideally the actuation-related modes have low frequencies due to high compliance, whereas the deformation modes should have high frequencies.

Table 1. Modeled eigenfrequencies with associated vibration modes.

| Mode | Frequency (rad/s) | Vibration motion* |
|---|---|---|
| 1 | 54.6 | end-effector translation in y'-direction |
| 2 | 55.2 | end-effector translation in x'-direction |
| 3 | 81.1 | end-effector rotation around z-axis |
| 4 | 83.3 | end-effector translation in z-direction |
| 5 | 119 | end-effector rotation around y'-axis |
| 6 | 122 | end-effector rotation around x'-axis |
| 7 | 624 | z-bending of in-plane leaf-springs |
| 8 | 787 | z-bending of in-plane leaf-springs |
| 9 | 836 | z-bending of in-plane leaf-springs |
| 10 | ≥944 | other (internal) modes of leaf-springs |

* The x'-y' axis system is rotated 45 degrees, with respect to the x-y axis system, around the z-axis.

## Control strategy

To obtain insight into the dynamical behavior of the mechanism, the transfers between actuator force and sensor displacement can be analyzed with help of the model; see Figure 4. Although the system is non-linear, for control purposes the system is linearized around the equilibrium configuration. The dominant character of the direct transfers between actuator force and sensor displacement, which was shown in analyses with the model, allows the use of a relatively simple single-input single-output (SiSo) control on every actuator-sensor pair separately. This results in a 6xSiSo controller for the whole system.

Each nominal SiSo model of the dominant transfer, with voltage as input and displacement as output, can be described by:

$$G_{nom_j} = \frac{\frac{k_m}{R}}{m_j s^2 + \frac{k_m k_v}{R} s + k_j}, \qquad (1.1)$$

where $k_m$ is the motor constant, $k_v$ the velocity constant, $R$ the coil resistance and $m_j$ and $k_j$ are the nominal mass and nominal stiffness per actuated direction respectively, and $j = 1...6$. These nominal models will be used for a controller design. As feedback controller type a PID-controller was chosen. Advantages of this type of controller are a good stability margin because of the D-action and a small setpoint error because of the I-action. The basic form of PID-control is:

$$G_{FB_j} = k_{p_j} \frac{R}{k_m} \frac{(s\tau_z + 1)(s\tau_i + 1)}{(s\tau_p + 1)s\tau_i}, \qquad (1.2)$$

with the design parameters given in Equation (1.3) based on loop-shaping [7] (where $j$ stands for the $j^{th}$ controller and hence actuator).

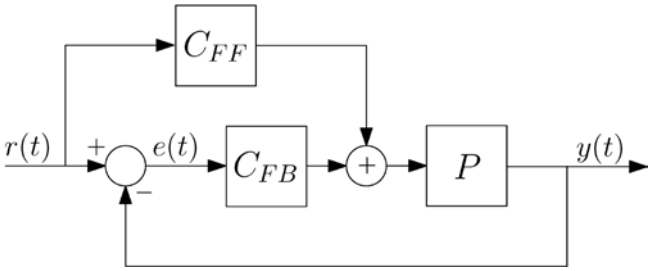


Figure 5. Closed loop with feedforward and feedback.

$$\begin{aligned} \tau_z &= \frac{\sqrt{1/\alpha}}{\omega_c} \\ \tau_i &= 2\cdot\tau_z \\ \tau_p &= \frac{1}{\sqrt{1/\alpha}\cdot\omega_c} \\ k_{p_j} &= \frac{m_j\cdot\omega_c^2}{\sqrt{1/\alpha}} \end{aligned} \tag{1.3}$$

where $\omega_c$ is the desired cross-over frequency of the open-loop, $\alpha$ a parameter between 0.1 and 0.2, namely the factor for the desired phase margin [7], $k_{p_j}$ the proportional gain of the controller, $\tau_i$ the corner point to stop integral action, $\tau_z$ the corner point to start derivative action and $\tau_p$ the corner point to stop derivative action – the corner point being the point in the Bode magnitude plot of a transfer function where the asymptote is turning into a line with a different angle.

However, using only feedback control will require a high cross-over frequency/bandwidth to reach the desired performance. Therefore, the reference signal is fed forward, filtered and added to the signal calculated by the feedback controller. In this way the feedback control is used for stability and disturbance rejection and the feedforward control is used to increase performance. The control structure is shown in Figure 5.

The optimal filter in the feedforward is equal to the inverse of the open-loop system model, which in this case leads to the following feedforward filter:

$$C_{FF_{jj}} = G_{nom_j}^{-1} = \frac{R}{k_m}\cdot\left(m_{jj}s^2 + \frac{k_m k_v}{R}s + k_{jj}\right) \tag{1.4}$$

where the left part, $R/k_m$, is the multiplication factor between voltage and force. Since using the model allows analysis of the non-dominant transfers as well, the elements outside the main diagonal of the feedforward filter matrix can be filled with stiffness parameters. This is valid, as the elements on the diagonal are dominant and represent the dynamics. The off-diagonal parameters are only used for static compensation. This leads to a feedforward filter matrix given in Equation (1.5), where $k_{ij}$ is the modeled nominal stiffness between actuator $i$ and $j$.

$$C_{FF_{ij}} = \begin{bmatrix} C_{FF_{11}} & \frac{-R}{k_m}\frac{k_{22}^2}{k_{12}} & \cdots & \frac{-R}{k_m}\frac{k_{66}^2}{k_{16}} \\ \frac{-R}{k_m}\frac{k_{11}^2}{k_{21}} & C_{FF_{22}} & \cdots & \frac{-R}{k_m}\frac{k_{66}^2}{k_{26}} \\ & \vdots & & \\ \frac{-R}{k_m}\frac{k_{11}^2}{k_{61}} & \frac{-R}{k_m}\frac{k_{22}^2}{k_{62}} & \cdots & C_{FF_{66}} \end{bmatrix} \tag{1.5}$$

To quantify the controller behavior, a measure for the tracking error was formulated, based on a skew sine as reference signal:

$$e_{tracking} = \frac{4\omega_r^2(1-\gamma)}{\alpha\omega_c^3}\frac{h_m}{t_m}, \tag{1.6}$$

in which $\omega_r$ is the resonance frequency, $\omega_c$ the required cross-over frequency, $\alpha$ a factor for the desired phase margin, $\gamma$ a factor for the expected model (un)certainty, $h_m$ the step size and $t_m$ the set-up time of the step of the reference. In case of a maximum tracking error according to the specifications (4 µm) this leads, combined with the parameters given in Table 2, to the requirement of $\omega_c$ = 323 rad/s.

Table 2. Control parameters.

| Parameter | Value | Unit |
|---|---|---|
| $e_{tracking}$ | ≤ $4\cdot10^{-6}$ | m |
| $\alpha$ | 0.1 | - |
| $\omega_r$ | 75 | rad/s |
| $r$ | 0.9 | - |
| $k_{p_j}$ | $8\cdot10^3$ – $9.1\cdot10^3$ | - |
| $m_j$ | 0.243-0.276 | kg |
| $h_m$ | $6\cdot10^{-3}$ | m |
| $t_m$ | 1 | s |

## Simulations

Simulink was used to simulate the closed-loop system in order to check the calculations. As a reference signal a skew sine with a step size of 3 mm with a set-up time of 1 second was used. The simulation results are shown in Figure 6. As can be seen the maximum tracking error is larger than in the calculations, where only one SiSo case was accounted for. This shows there is some amount of crosstalk which cannot be ignored, but which is small enough to make 6xSiSo control possible.

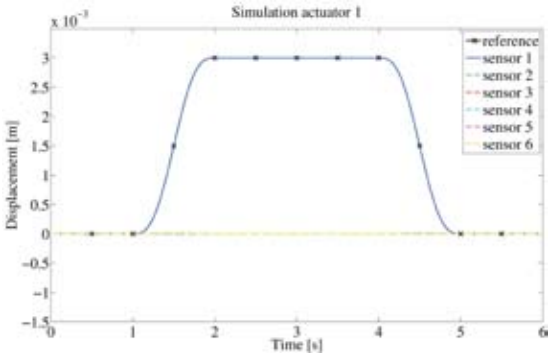


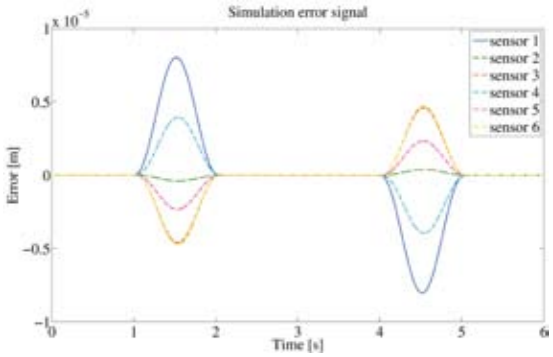


Figure 6. Simulation of the complete system.
(a) One actuator was being fed a non-zero reference signal. (b) Tracking errors.

Furthermore, these simulations show that the maximum tracking error occurs at the actuator with the non-zero reference signal. This is because the feedforward is designed in SiMo mode, where the reference signal of one actuator is forwarded to all actuators through the modeled stiffness of the mechanism.

## Experimental validation

To validate the calculations and simulations a functional set-up, Figure 7, was built. In this set-up voice-coil actuators were used. Besides these actuators, linear variable differential transducer (LVDT) sensors were used. These actuators and sensors are connected to their amplifiers and signal conditioning electronics, respectively, which are each connected to a dSpace 1103 interface board. At this interface board six digital-to-analog and six analog-to-digital ports were used.

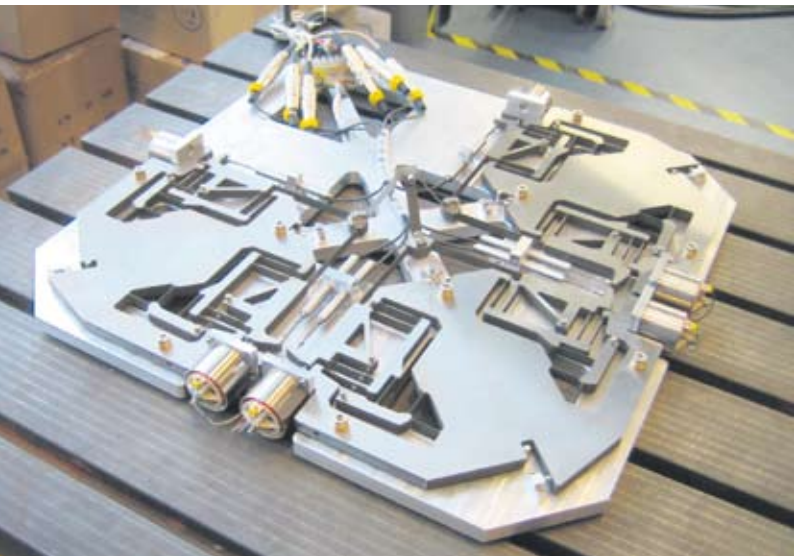

Figure 7. Experimental set-up.

## Identification

Figure 8 shows the experimentally determined frequency responses between actuator 1 and all sensors. As can be seen at first glance, the transfers resemble the transfers predicted by SPACAR (Figure 4).

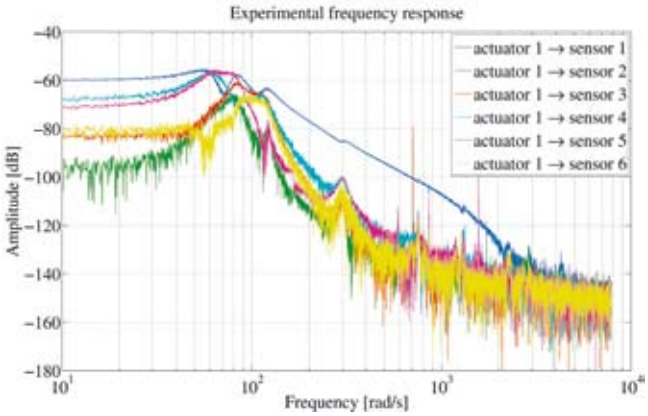


Figure 8. Experimentally determined frequency responses.

A closer inspection leads to the frequencies given in Table 3, completed with the relative errors between the values from experiment and model. As can be seen the relative error of the seventh to ninth frequency is larger than that of the lower frequencies. This can be explained by fabrication tolerances. The difference is probably caused by the non-uniform dimensions of the wire spark eroded leaf-springs, which are slightly different compared to the specification. The other peaks visible are introduced by the electronics used. The first highly damped peak at 314 rad/s (≈50 Hz) is caused by the AC power which is used by all electronics.

Table 3. Experimentally determined eigenfrequencies with their relative error.

| Mode | Eigenfrequency | | Error (%) |
|---|---|---|---|
| | Model (rad/s) | Exp. (rad/s) | |
| 1 | 54.6 | 55.8 | 2.2 |
| 2 | 55.2 | 57.0 | 3.3 |
| 3 | 81.1 | 80.2 | 1.1 |
| 4 | 83.3 | 85.2 | 2.3 |
| 5 | 119 | 118 | 1.2 |
| 6 | 122 | - | - |
| 7 | 624 | 589 | 5.9 |
| 8 | 787 | 753 | 4.5 |
| 9 | 836 | 800 | 4.5 |

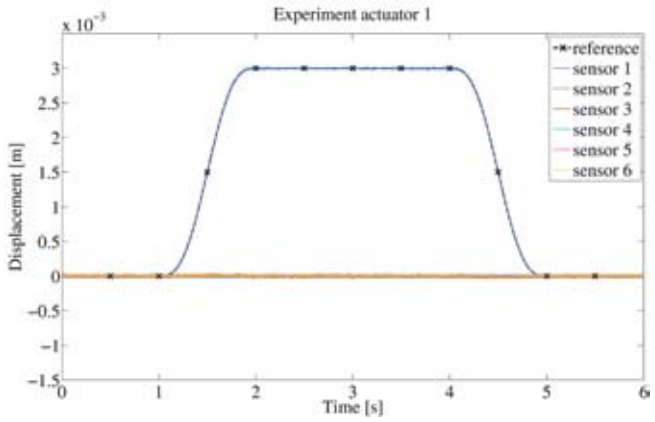


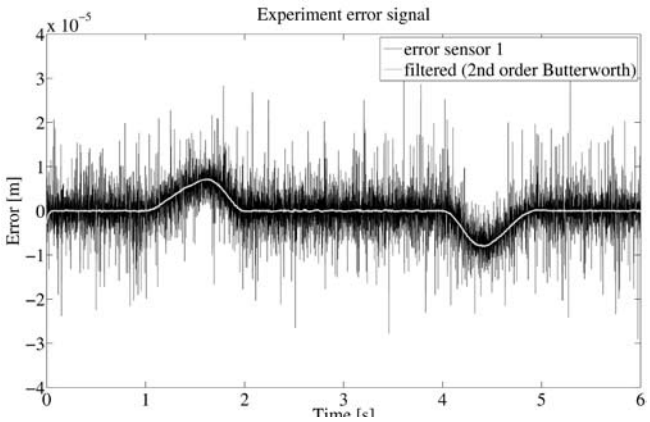


Figure 9. Experimental results of the complete system.
(a) One actuator was being fed a non-zero reference signal.
(b) Error signal.

## Closed-loop experiments

Once the frequency responses of the prototype are known, the designed controller can be tested in practice. From comparing the modeled transfers (Figure 4) to the estimated frequency responses (Figure 8) it can be concluded that the model seems to resemble the prototype very well. Therefore, the frequency responses modeled by SPACAR are assumed to be valid. This has the advantage that the previously designed controllers do not have to be modified and can be integrated directly.

In the experiments again one actuator was given a skew sine reference signal, and the other actuators were given a zero reference signal. The result of an experiment with a step size of 3 mm is shown in Figure 9a (positive displacement is outward). This figure shows that the system behaves as expected. However, a large signal variance is observed for the actuators which are kept at zero displacement. This is mainly due to the noise generated by the sensors.

When the error of actuator 1 is inspected in detail (Figure 9b) it can be seen that the tracking error is in accordance with previous simulations. The other error signals show a behavior comparable to the simulations performed; hence, they are not given.

## Conclusions

In this article the design, modeling and control of a scaled-up elastic parallel kinematic 6-DOFs manipulator has been discussed. The model created with the SPACAR toolbox showed a great resemblance with the prototype. Identification experiments showed an error between prototype and linearized model of the first six eigenfrequencies below 3.5% and the error of the seventh to ninth just below 6%. This difference can be caused by dimensions of the wire spark eroded leaf-springs that are slightly different compared to specification, due to fabrication tolerances.

Furthermore, simulations performed with the model were validated with experiments at the prototype. This comparison showed the model is relatively accurate. Therefore, the SPACAR model is assumed to be adequate and applicable for model-based controller design.

## Authors' note

Martijn Huijts is a mechanical designer at MI-Partners in Eindhoven, the Netherlands. The work described in this article was part of his Master's thesis at the University of Twente. Dannis Brouwer and Johannes van Dijk are assistant professors in the department of Mechanical Engineering at the University of Twente, Enschede, the Netherlands. Dannis Brouwer is also project manager with DEMCON in Oldenzaal, the Netherlands.

## References

[1] Brouwer, D.M., et al., Design and modeling of a six DOFs MEMS-based precision manipulator. *Precis Eng* (2009), doi:10.1016/j.precision eng.2009.08.001, in press.
[2] Blanding, D.L., "Exact constraint: Machine design using kinematic processing", ASME press, New York, 1999, ISBN 0-791-80085-7.
[3] M.P. Koster, "Constructieprincipes voor het nauwkeurig bewegen en positioneren", Twente University Press, 2000, ISBN 903651455x.
[4] Meijaard, J.P., Brouwer, D.M., Jonker, J.B., Analytical and experimental investigation of a parallel leafspring guidance, *Multibody Syst. Dyn.*, doi:10.1007/s11044-009-9172-4, 2009.
[5] The SPACAR software package, 2009; see also www.spacar.nl.
[6] Jonker, J.B., Aarts, R.G.K.M., van Dijk, J., A linearized input-output representation of flexible multibody systems for control synthesis. *Multibody Syst. Dyn.*, vol. 21, no 2, pages 99–122, 2009.
[7] Van Dijk, J., "Systeem- en regeltechniek 2", University of Twente, 2009.